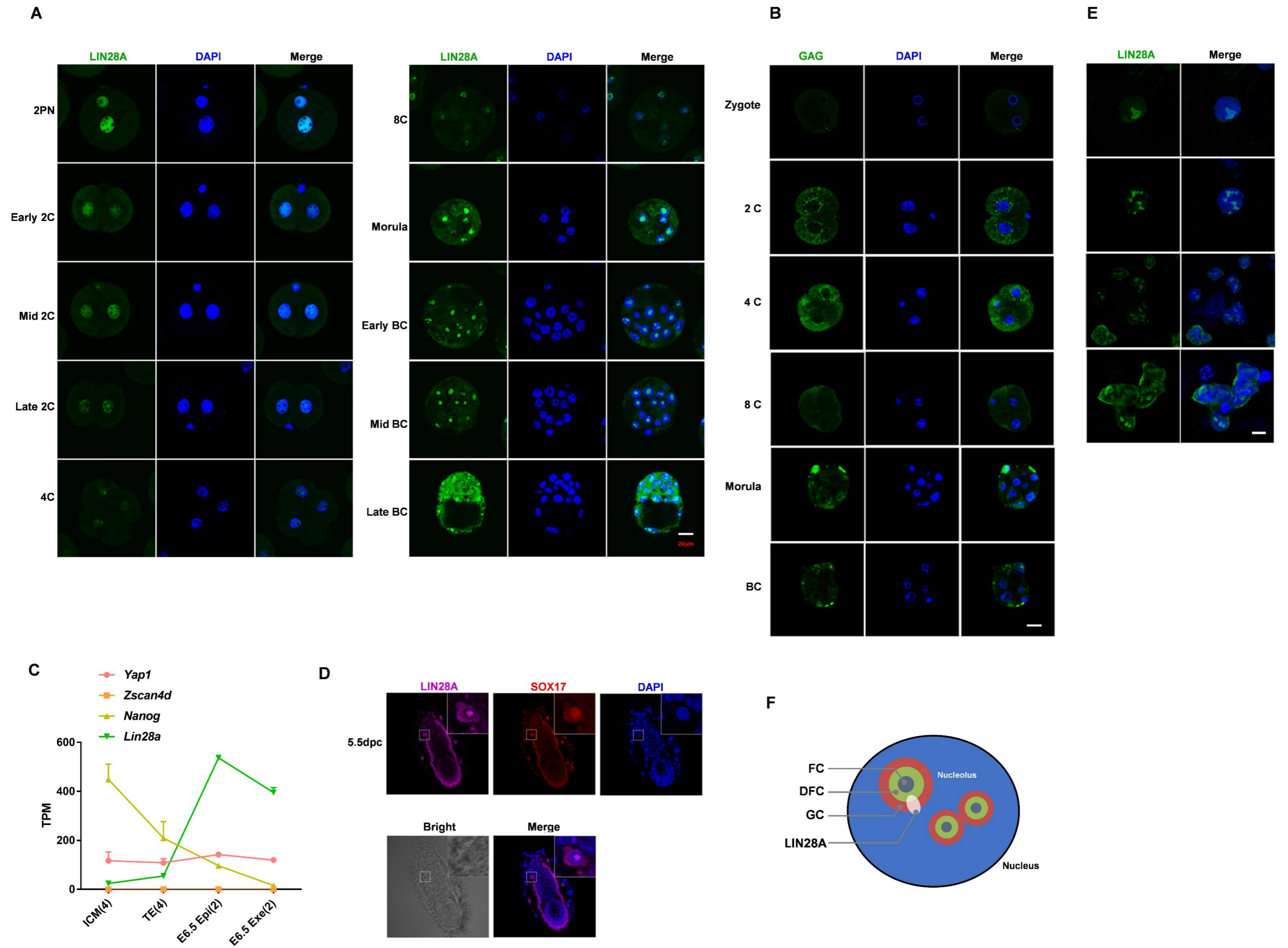


Supplementary Figures for

**LIN28 Coordinately Promotes Nucleolar/Ribosomal Functions and Represses the 2C-like Transcriptional Program in Pluripotent Stem Cells**

Zhen Sun<sup>1, #</sup>, Hua Yu<sup>1, #</sup>, Jing Zhao<sup>1, #</sup>, Tianyu Tan<sup>1</sup>, Hongru Pan<sup>1</sup>, Yuqing Zhu<sup>1</sup>, Lang Chen<sup>1</sup>, Cheng Zhang<sup>2</sup>, Li Zhang<sup>1</sup>, Anhua Lei<sup>1</sup>, Yuyan Xu<sup>1</sup>, Xianju Bi<sup>3</sup>, Xin Huang<sup>4</sup>, Cristina Correia<sup>2</sup>, Ming Chen<sup>5</sup>, Qiming Sun<sup>6</sup>, Li Shen<sup>7</sup>, Jianlong Wang<sup>4</sup>, Xiaohua Shen<sup>3</sup>, George Q. Daley<sup>8</sup>, Hu Li<sup>2</sup>, Jin Zhang<sup>1,9\*</sup>

Figure S1



**Fig. S1. Temporal and spatial expression of LIN28A in mouse early embryo development. Related to Fig. 1.**

(A) LIN28A immunostaining at indicated differentiation stages. Scale bar, 20  $\mu\text{m}$ .

(B) Gag protein expression assessed by immunostaining during mouse early embryo development. Scale bar, 20  $\mu\text{m}$ .

(C) Lin28a mRNA expression in post-implantation embryos analyzed from published RNA-seq data (Wang, et. al., 2018). Numbers in the parentheses mean the number of embryos.

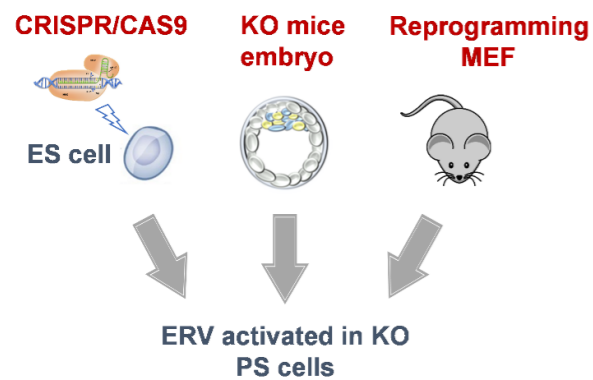
(D) Immunostaining showing LIN28A protein expression in post-implantation embryos.

(E) Lin28A immunostaining in single pluripotent stem cell and small colonies. Scale bar, 10  $\mu\text{m}$ .

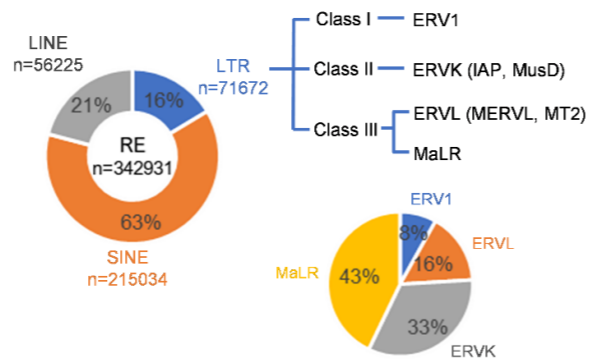
(F) Cartoon illustrating three nucleolar compartments and Lin28A's localization in the nucleus. GC (granular component), DFC (dense fibrillar component), and FC (fibrillar center).

**Figure S2**

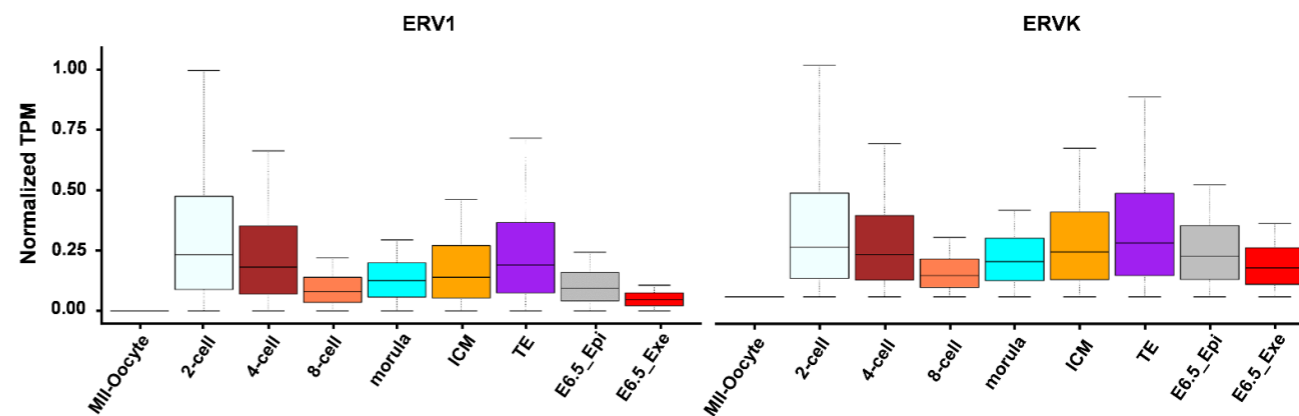
**A**



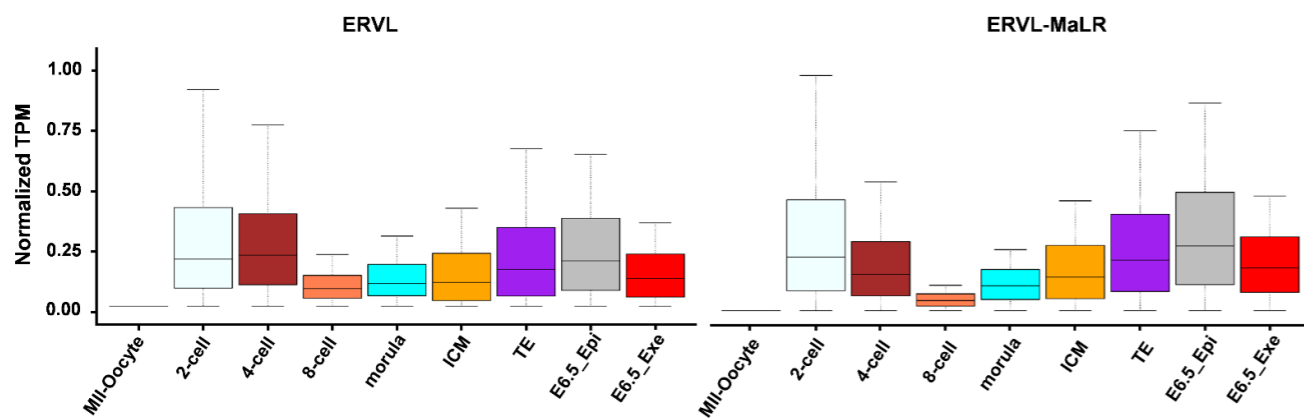
**B**



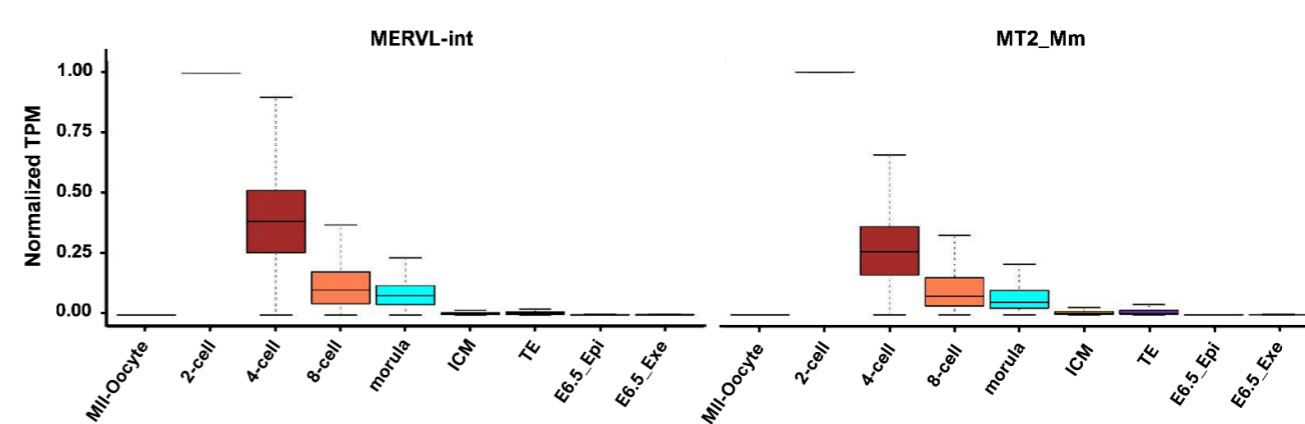
**C**



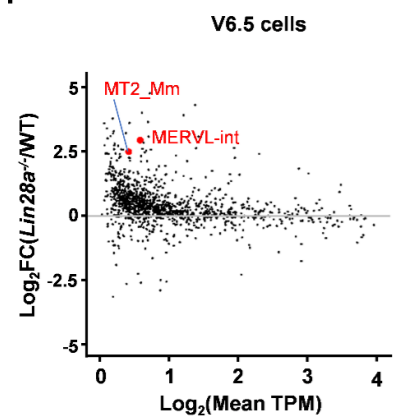
**D**



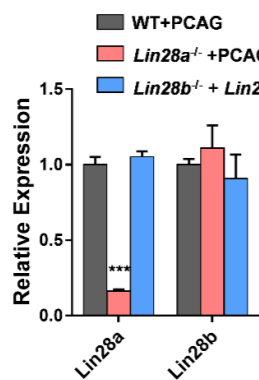
**E**



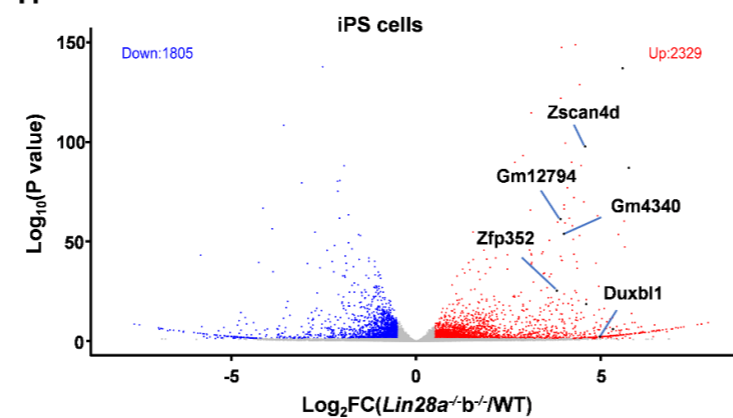
**F**



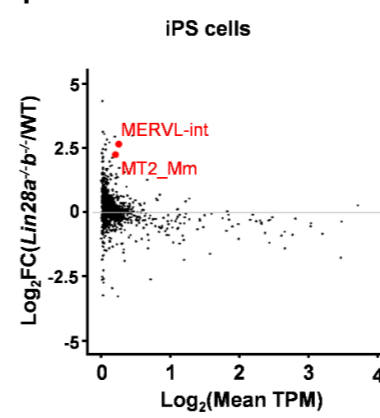
**G**



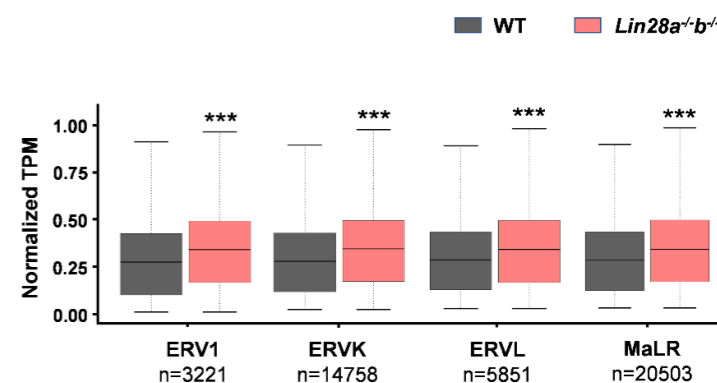
**H**



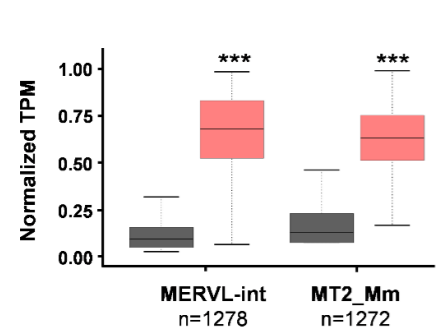
**I**



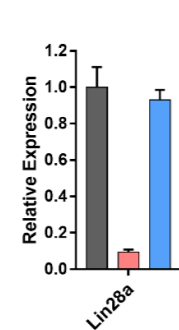
**J**



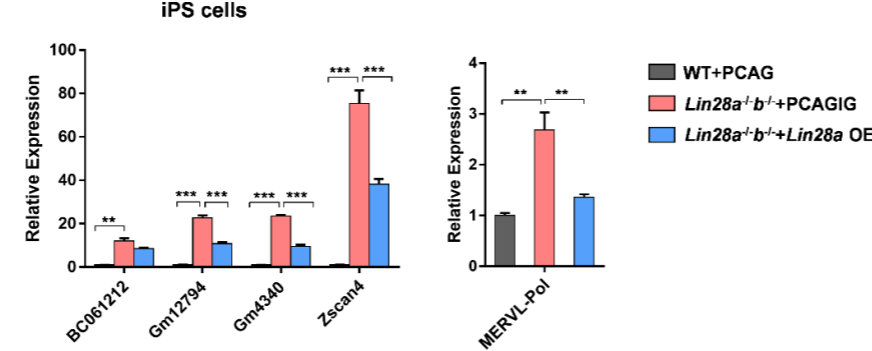
**K**



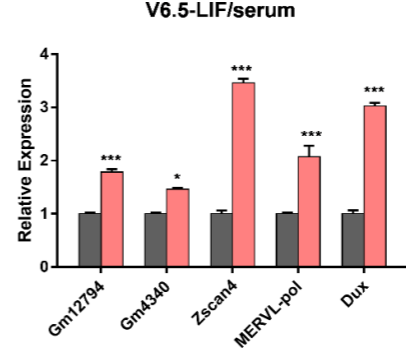
**L**



**M**



**N**



**O**

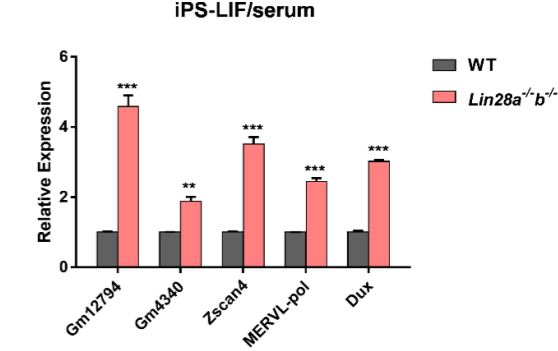


**Fig. S2. LIN28 double knockout causes activation of ERV and 2C marker genes in iPS cells. Related to Fig. 2.**

(A) A summary of three independent methods used to generate LIN28-deficient PS cells.

(B) Classification of transposable elements.

(C, D) Expression of different classes of ERV across different embryo developmental stages. The TPM values of LTR expression were linearly normalized to a range from 0 to 1 across all samples.

(E) Expression of two MERVL sub-classes MERVL-int and MT2\_Mm in different embryo developmental stages. The TPM values of LTR expression were linearly normalized to a range from 0 to 1 across all samples.

(F) MA plot showing log<sub>2</sub>-fold changes in repeat sequence gene expression following Lin28a knockout in ES cells. Upregulated MERVL repeats are indicated.

(G) qRT-PCR showing Lin28a/b expression in the indicated conditions in ES cells.

(H) Volcano plot of RNA-seq showing alterations of gene expression upon Lin28a/b double knockout in iPS cells. Typical 2C genes are highlighted.

(I) MA plot showing log<sub>2</sub>-fold changes in repeat sequence gene expression following Lin28a/b double knockout in iPS cells.

(J) Different classes of Long Terminal Repeat or LTR expression in Lin28a/b double knockout iPS cells. The TPM values of LTR expression were linearly normalized to a range from 0 to 1 across all samples. \*\*\*:  $p < 0.001$ , Wilcoxon signed rank test.

(K) Two sub-classes of MERVL genes MERVL-int and MT2\_Mm expression in Lin28a/b double knockout iPS cells. The TPM values of LTR expression were linearly normalized to a range from 0 to 1 across all samples. \*\*\*:  $p < 0.001$ , Wilcoxon signed rank test.

(L, M) qRT-PCR showing Lin28a (L), 2C genes and MERVL expression (M) in the indicated conditions in iPS cells.

(N, O) qRT-PCR showing the expression of 2C-related genes in wild-type and Lin28a knockout ES cells (N) and Lin28a/b double knockout iPS cells (O) cultured in LIF/serum medium for 7 days. For (N-P), \*:  $p < 0.05$ , \*\*:  $p < 0.01$ , \*\*\*:  $p < 0.001$ , two-way ANOVA,  $n=3$ , error bar: standard error of the mean.

**Figure S3**

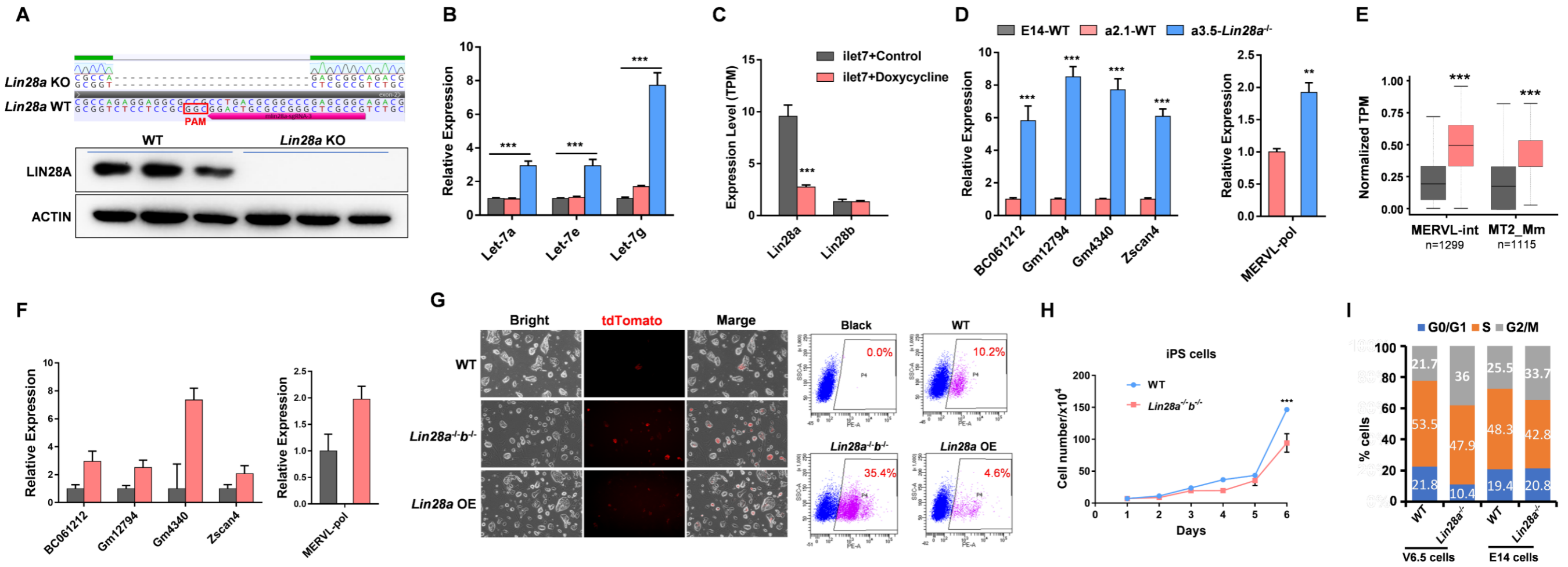


**Fig. S3. The increase of 2C marker genes and decrease of cell proliferation in *Lin28* deficiency cells. Related to Fig. 2.**

- (A) Sanger sequencing analysis and western blotting showing LIN28A protein knockout with CRISPR/CAS9 from multiple clones.
- (B) qRT-PCR showing let-7 expression in un-transfected E14 ES cells, transfected wild-type clone a2.1 and CRISPR/CAS9 knockout clone a3.5.
- (C) 2C gene and ERV expression in the same conditions as in (B).
- (D) qRT-PCR showing Lin28 mRNA level in untreated and 3-day doxycycline-treated inducible let-7 (*ilet7*) ES cells. \*:  $p < 0.05$ , \*\*:  $p < 0.01$ , \*\*\*:  $p < 0.001$ , two-way ANOVA,  $n=3$ , error bar: standard error of the mean.
- (E) Analysis of RNA-seq showing two classes of MERVL genes MERVL-int and MT2\_Mm are up-regulated in let-7 overexpressing ES cells. The TPM values of LTR expression were linearly normalized to a range from 0 to 1 across all samples. \*\*\*:  $p < 0.001$ , Wilcoxon signed rank test.
- (F) qRT-PCR showing 2C genes and ERV genes in let-7 overexpressing ES cells.
- (G) Microscopy picture and flow cytometry data showing proportion of 2C-like cells using iPS cells transduced with a 2C::tdTomato reporter construct.
- (H) Cell proliferation curve for wild-type and Lin28a/b double knockout iPS cells. \*\*\*:  $p < 0.001$ , two-way ANOVA,  $n=3$ , error bar: standard error of the mean.
- (I) Summary of cell cycle analysis across various conditions of Lin28 knockout cells and wild-type cells using PI staining and flow cytometry.

Figure S4

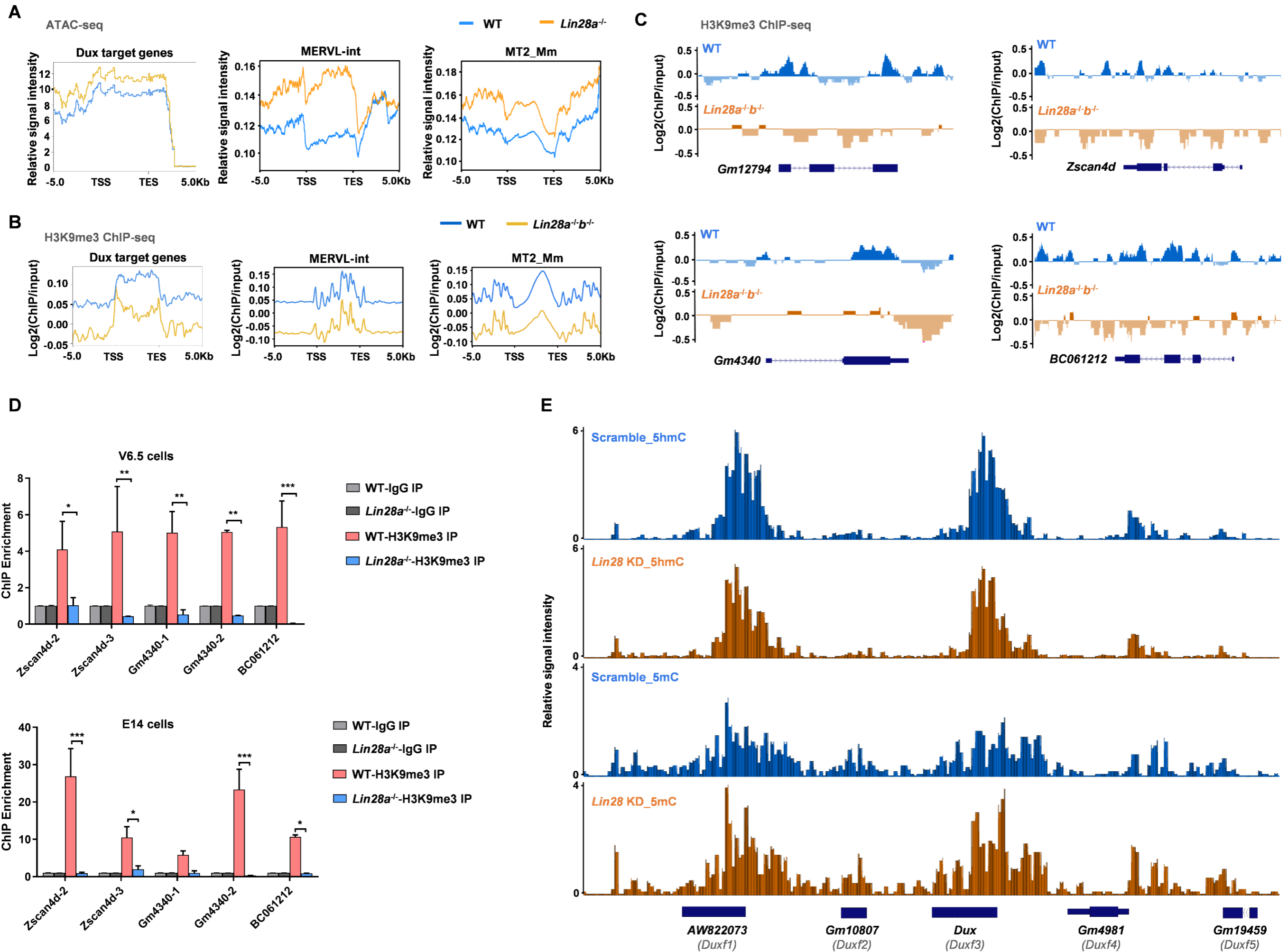


**Fig. S4. The epigenetic modification of Dux targets. Related to Fig. 3.**

- (A) ATAC-seq peaks in the proximity of the Dux target genes, MERVL-int and MT2\_Mm ERVs in wild-type and knockout ES cells.
- (B) ChIP-seq showing local H3K9me3 level in the proximity of Dux target genes, MERVL-int and MT2\_Mm classes of ERVL genes in wild-type and double knockout iPS cells.
- (C) UCSC Genome Browser view of ChIP-seq results for representative Dux targets 2C genes in wild-type and double knockout iPS cells.
- (D) ChIP-PCR showing H3K9me3 levels of 2C genes in wild-type and CRISPR/CAS9 generated knockout V6.5 (left panel) or E14 ES cells (right panel).
- (E) MeDIP-seq and 5hmC-seq showing levels of DNA methylation and hydroxymethylation in the proximity of Dux family genes in wild-type and Lin28a knockout ES cells. \*:  $p < 0.05$ , \*\*:  $p < 0.01$ , \*\*\*:  $p < 0.001$ , two-way ANOVA,  $n=3$ , error bar: standard error of the mean.

Figure S5

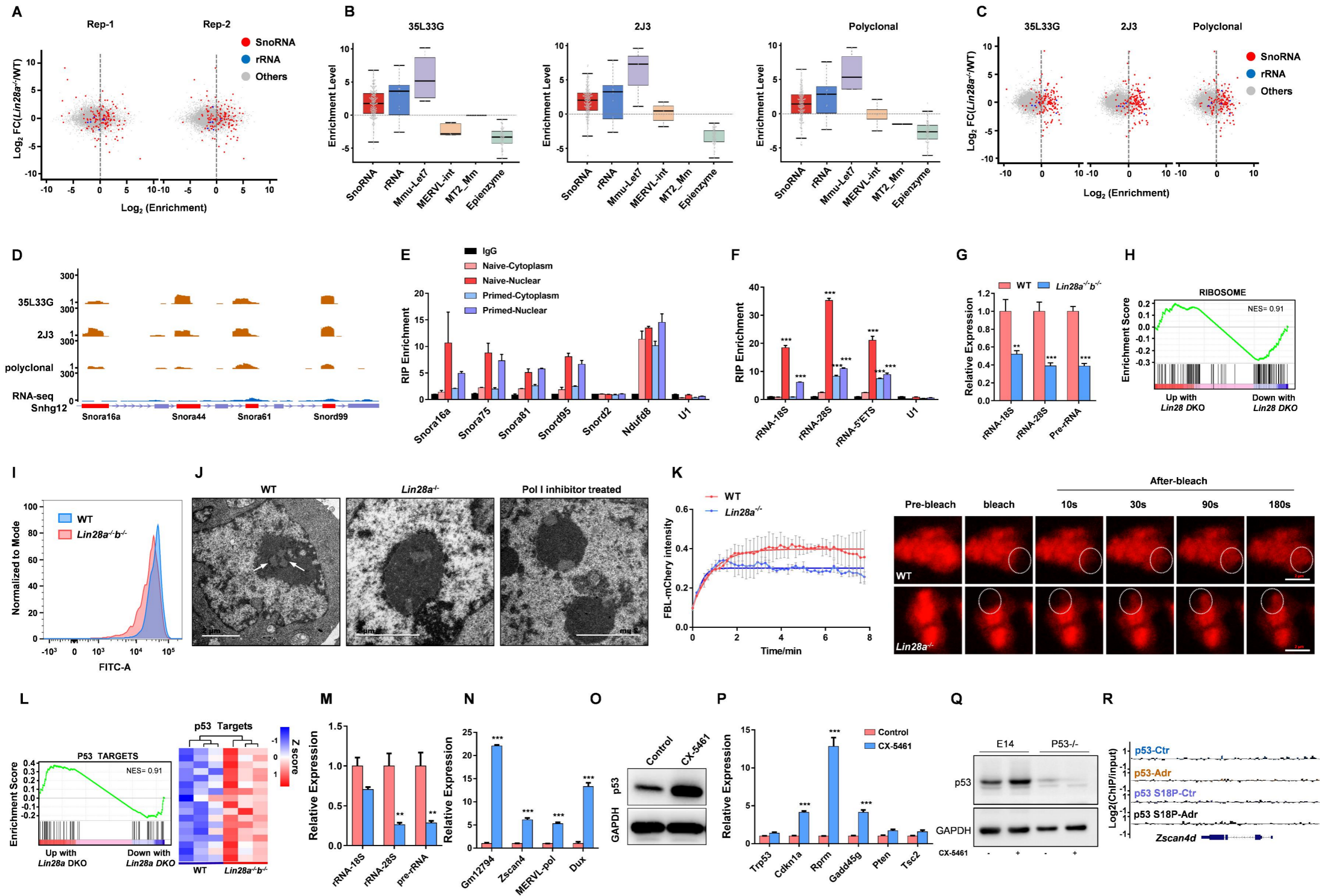


**Fig. S5. Lin28 deficiency leads to nucleolar abnormalities. Related to Fig. 4.**

(A) Enrichment of LIN28A binding targets and fold change expression between Lin28a knockdown and scramble are plotted for snoRNA, rRNA and all other genes.

(B) Analysis of published CLIP-seq data (Cho et. al., 2012) with three different LIN28A antibodies (35L33G, 2J3 and Polyclonal antibodies) showing enrichment of binding to indicated RNA. Let7 was used as positive control.

(C) Enrichment of LIN28A binding targets and change expression between Lin28a knockdown and scramble (Cho et. al., 2012) are plotted for snoRNA, rRNA and all other genes.

(D) An example of LIN28 binding signal derived from CLIP-seq at the indicated snoRNA locus.

(E) RIP-qPCR showing LIN28 binding to snoRNAs, as well as its cytoplasmic binding target Ndufd8 in the naïve and primed ES cells.

(F) RIP-qPCR analysis of LIN28A binding to rRNA in the naïve and primed ES cells.

(G) qRT-PCR showing the expression of pre- and mature rRNA in wild-type and Lin28a/b double knockout iPS cells.

(H) GSEA analysis showing collective changes in the ribosomal protein gene set of Lin28a/b double knockout iPS cells versus wild-type cells.

(I) Flow cytometry showing OP-puromycin labeling of wild-type and Lin28a/b double knockout iPS cells.

(J) Electro-microscopy showing nuclear morphology of wild-type and Lin28a knockout E14 ES cells.

(K) Left panel: Normalized fluorescence intensity in wild-type and Lin28 knockout cells stably expressing FBL-mCherry with FRAP analysis. Right panel, representative time-lapse images of pre-bleaching, immediately after bleaching (Bleach) and the first 180 s after bleaching were shown. Curves are given as mean values  $\pm$  SD; n = 4 biological repeats representing at least 9 different cells.

(L) Left panel: GSEA analysis showing collective changes in the p53 pathway gene set of Lin28a/b double knockout iPS cells versus wild-type cells. Right panel: up-regulation of p53 pathway genes in Lin28a/b double knockout iPS cells compared with wild-type cells.

(M) qRT-PCR showing the expression of 18S, 28S and pre-rRNA in ES cells treated with 4  $\mu$ M Pol I inhibitor (CX-5461) for 12 hr or equal water (control).

(N) qRT-PCR showing 2C gene expression in ES cells treated with 4  $\mu$ M Pol I inhibitor (CX-5461) for 12 hr or equal water (control).

(O) Western blotting showing activation of p53 with treatment of CX-5461 or Nutin3 as a control.

(P) qPCR showing p53 target expression upon CX-5461 treatment.

(Q) Western blotting showing p53 protein level upon treatment in wild-type and p53 knockout cells.

(R) UCSC Genome Browser view of ChIP-seq results using antibodies of p53 and phosphorylated p53 S18P for Zscan4d gene locus. \*: p<0.05, \*\*: p<0.01, \*\*\*: p<0.001, two-way ANOVA, n=3, error bar: standard error of the mean.

**Figure S6**

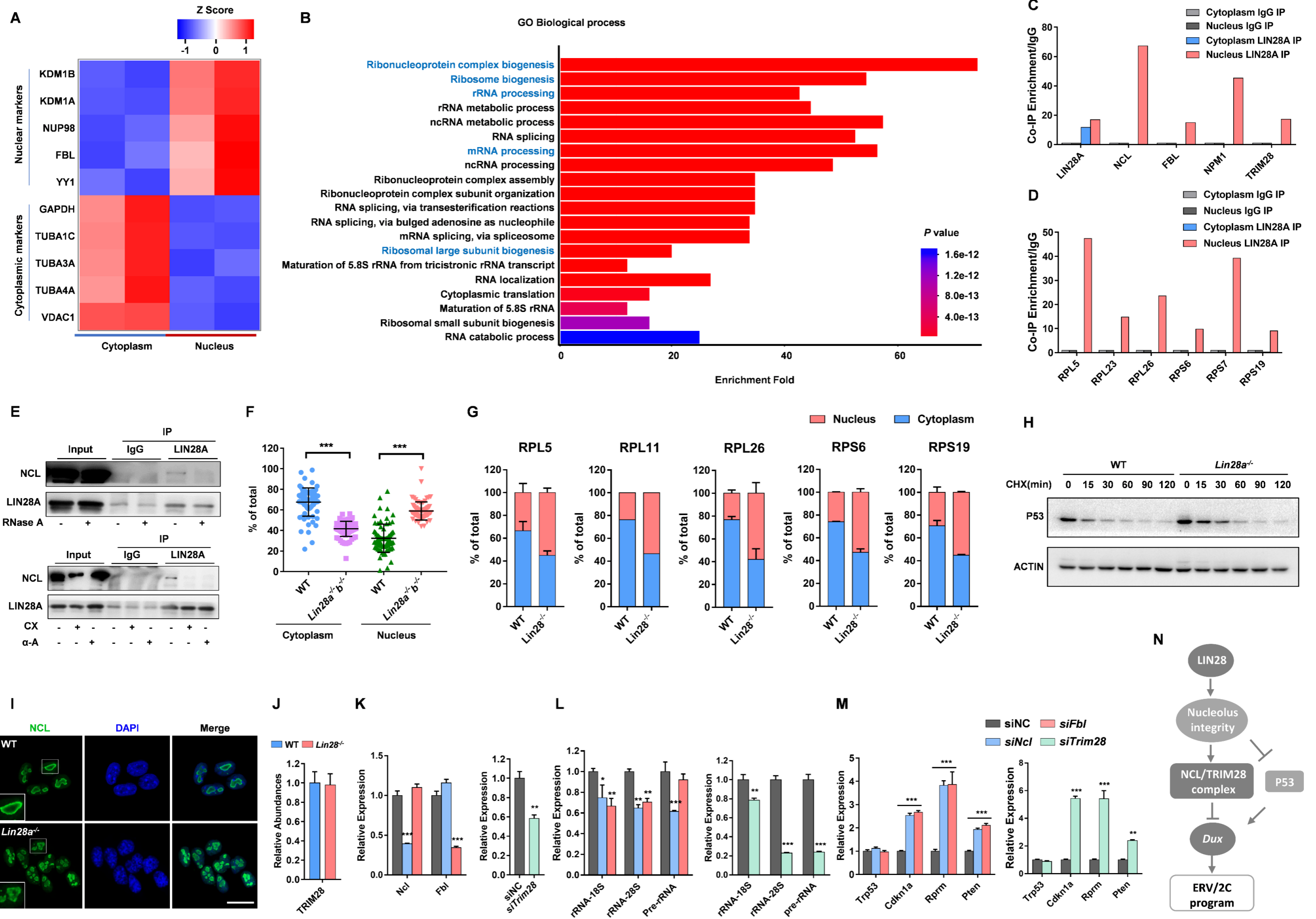


**Fig. S6. *Lin28* interacts with nucleolar proteins and regulates *Dux* expression through the NCL/TRIM28 complex. Related to Fig. 5.**

(A) Heatmap showing that cytosol and nucleus fractions were separated for proteomics analysis.

(B) GO analysis of proteins pulled down by the LIN28A antibody.

(C, D) Co-immunoprecipitation (Co-IP) showing the interaction between endogenous LIN28A and nucleolus proteins (C) and ribosomal proteins (D) in ES cells by mass spectroscopy.

(E) Co-IP showing association of endogenous LIN28A and NCL proteins in ES cells treated with RNase A (100 µg/ml for 30 min at 37 °C, upper panel) or Pol I inhibitor (4 µM CX-5461 for 12 hr), Pol II inhibitor (10 µg/ml α-Amantin for 12 hr) (lower panel) by Western blotting.

(F, G) Proteomics analysis showing the nucleus and cytoplasm proportion of all ribosomal proteins (F) and indicated proteins (G) in wild-type and *Lin28* knockout cells. (G) is the average of *Lin28a* knockout ES cells and *Lin28a/b* knockout iPS cells. \*\*\*:  $p < 0.001$ , t-test, error bar: standard error of the mean. Error bar in (G) means standard error of the mean of 2 independent proteomics experiments from ES and iPS cells.

(H) Western blot showing p53 protein half-life in wild-type and *Lin28a* knockout ES cells treated with 100 µg/ml of cycloheximide (CHX).

(I) Immunofluorescence staining of NCL in wild-type and *Lin28a/b* double knockout iPS cells. Scale bar, 20 µm.

(J) Proteomics analysis showing the relative abundances of TRIM28 proteins in wild-type and *Lin28* knockout cells (averaged proteomics data from *Lin28a* knockout ES cells and *Lin28a/b* knockout iPS cells). Error bar: standard error of the mean.  $n=2$  independent proteomics experiments.

(K-M) qRT-PCR showing the mRNA levels of indicated genes in ES cells transfected with scramble negative control or siRNAs against *Ncl*, *Fb* or *Trim28*. \*:  $p < 0.05$ , \*\*:  $p < 0.01$ , \*\*\*:  $p < 0.001$ , two-way ANOVA,  $n=3$ , error bar: standard error of the mean.

(N) Schematic illustration showing LIN28 regulates *Dux* expression through the nucleolus and NCL/TRIM28 complex.

**Figure S7**

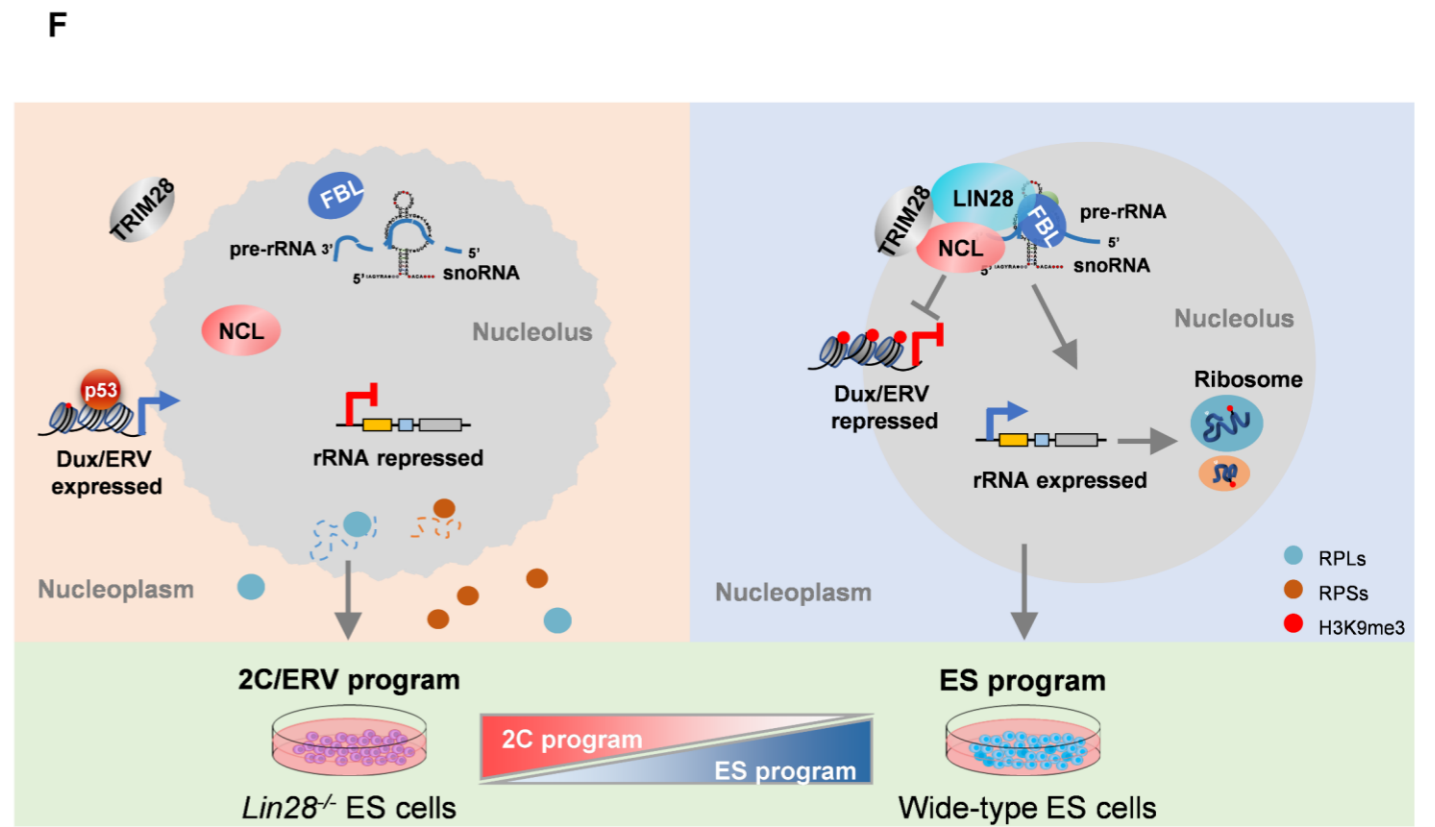
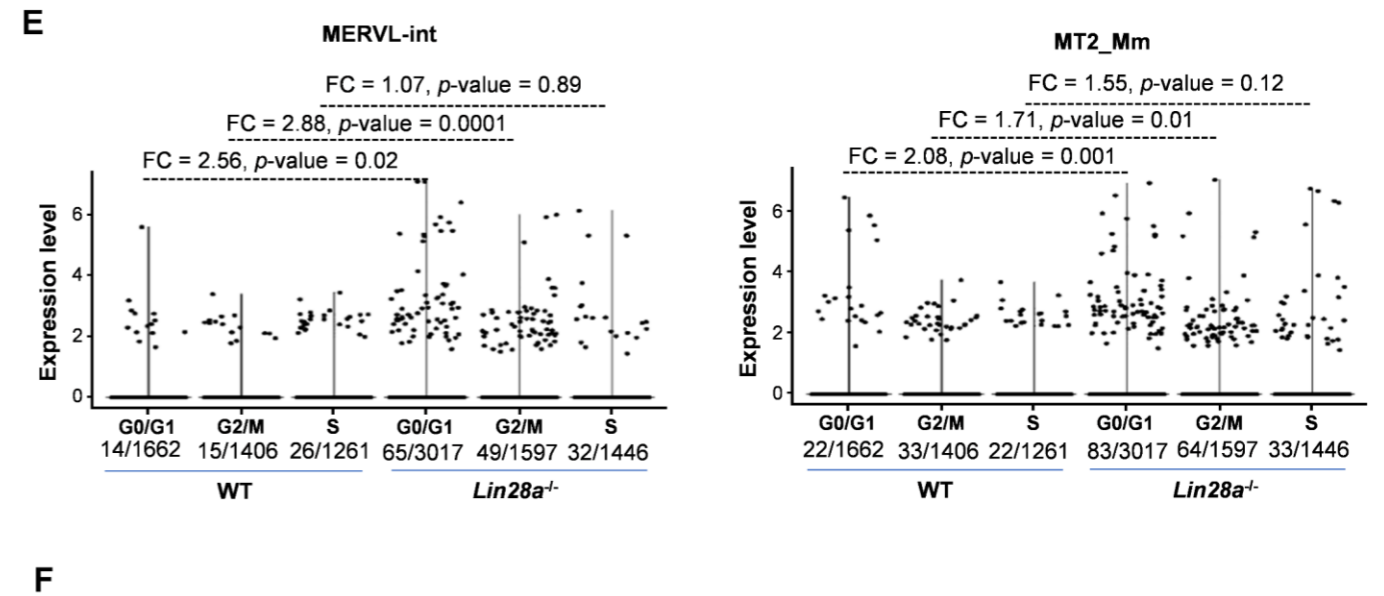
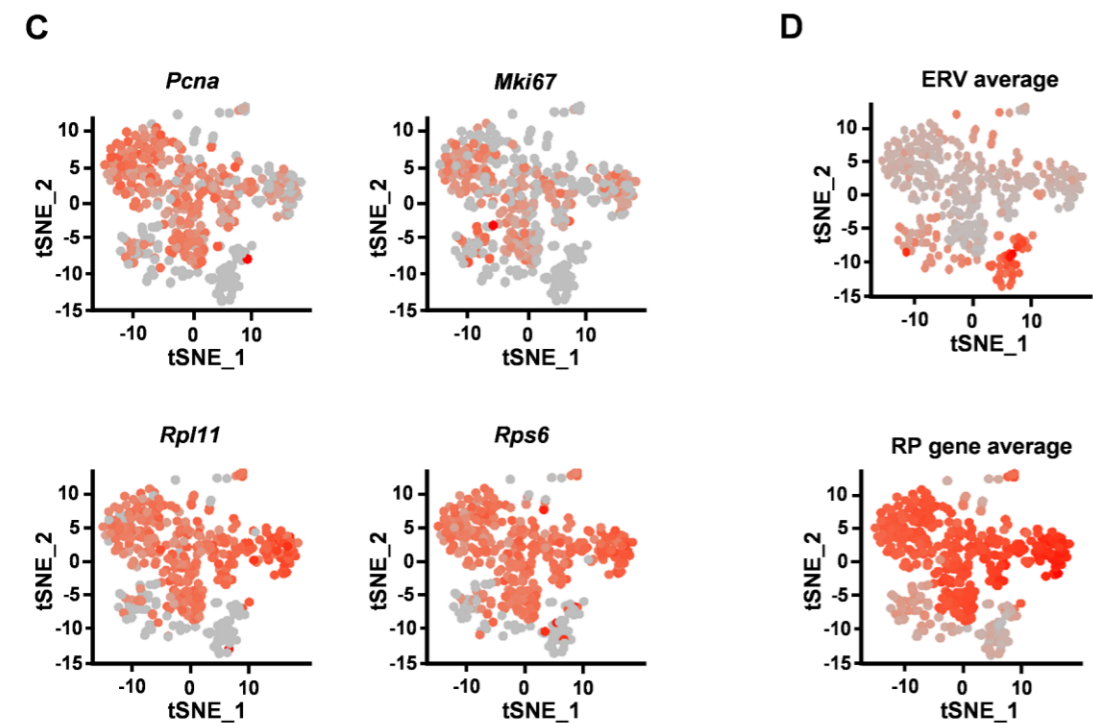
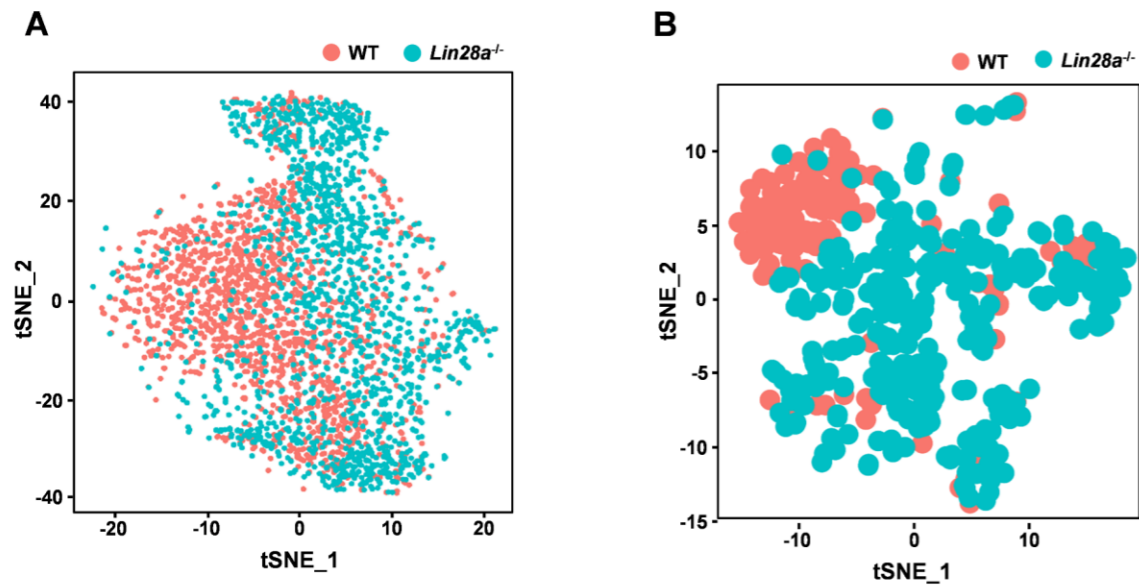


**Fig. S7. Single cell RNA-seq analysis of wild-type and *Lin28* knockout ES cells. Related to Fig. 6.**

(A) Single cell RNA-seq analysis and tSNE plot showing clustering of wild-type and *Lin28* knockout ES cells.

(B) tSNE plot showing clustering of wild-type and *Lin28* knockout ES cells filtered to only leave those with detected ERV expression.

(C) tSNE plots showing indicated gene expression with cells filtered to only leave those with detected ERV expression.

(D) tSNE plots showing averaged ERV or RP gene expression with cells filtered to only leave those with detected ERV expression.

(E) Single cell RNA-seq analysis showing cell cycle phase distribution of those cells expressing MERVL-int or MT2\_Mm in wild-type and *Lin28a* knockout ES cells. Each dot represents a single cell. The numbers below reflect the percentage of cells with ERV detected in each cell cycle phase. FC: fold changes of the number of cells in a certain cell cycle phase between knockout and wild-type cells. Fold changes for G0/G1 and G2/M phases are significant, but not for S phase. The p-values were calculated by Fisher's exact test.

(F) Schematic illustration showing LIN28 regulates nucleolar functions to coordinate 2C and ES cell programs. In the wild-type ES cell program, LIN28 in the nucleolus resides in the same complex with NCL/TRIM28 or in the liquid phase with other nucleolar RNAs and RNA binding proteins, and mediates NCL/TRIM28 occupancy on the Dux locus to repress Dux expression. Meanwhile, LIN28 also facilitates the same complex/liquid phase to promote rRNA expression and ribosome biogenesis. In contrast, in the *Lin28* knockout ES cells, as the LIN28-mediated complex is interrupted, Dux repression is released and rRNA expression is reduced which both contribute to the 2-cell like cell program. Nucleolar stress also activates p53 which can directly bind to Dux locus and promotes Dux expression.